Quasi-elastic scattering in the ^{20}Ne + ^{90,92}Zr reactions: Role of noncollective excitations

S. Yusa,[1] K. Hagino,[1] and N. Rowley[2]
[1]*Department of Physics, Tohoku University, Sendai 980-8578, Japan*
[2]*Institut de Physique Nucléaire, UMR 8608, CNRS-IN2P3 et Université de Paris Sud, 91406 Orsay Cedex, France*
(Received 18 September 2013; published 27 November 2013)

Conventional coupled-channels analyses, that take account of only the collective excitations of the colliding nuclei, have failed to reproduce the different behavior of the experimental quasi-elastic barrier distributions for the ^{20}Ne + ^{90,92}Zr systems. To clarify the origins of this difference, we investigate the effect of noncollective excitations of the Zr isotopes. Describing these excitations in a random-matrix model, we explicitly take them into account in our coupled-channels calculations. The noncollective excitations are capable of reproducing the observed smearing of the peak structure in the barrier distribution for ^{20}Ne + ^{92}Zr, while not significantly altering the structure observed in the ^{20}Ne + ^{90}Zr system. The difference is essentially related to the closed neutron shell in ^{90}Zr.

DOI: 10.1103/PhysRevC.88.054621 PACS number(s): 24.10.Eq, 25.70.Bc, 24.60.−k, 21.10.Pc

I. INTRODUCTION

In heavy-ion reactions around the Coulomb barrier, the relative motion between the projectile and the target nuclei couples to the internal degrees of freedom of the colliding nuclei in a decisive way, leading to a distribution of potential-barrier heights around the energy of the uncoupled Coulomb barrier [1]. This leads to the strong enhancements of sub-barrier fusion cross sections observed in a number of medium-heavy systems [2–4], when compared with the predictions of a simple potential model. The distribution of potential barriers $D_{\rm fus}$ can be obtained from measured fusion cross sections $\sigma_{\rm fus}(E)$ by taking the second derivative $D_{\rm fus} = d^2(E\sigma_{\rm fus})/dE^2$ with respect to the incident energy E [2,5,6]. The resulting fusion barrier distributions often exhibit structures [2,6,7] that are characteristic of the details of the collective states to which the entrance channel can couple.

It has been recognized that the concept of a barrier distribution can also be applied to cross sections for heavy-ion quasi-elastic scattering (that is, to the sum of elastic and inelastic scattering and transfer cross sections) [8,9]. For these processes, one can extract the barrier distribution from the measured total differential cross section $\sigma_{\rm qel}(\theta)$ at backward angles using the simple formula $D_{\rm qel} = -d(\sigma_{\rm qel}/\sigma_{\rm R})/dE$. Notionally, $\sigma_{\rm qel}$ and the Rutherford cross section $\sigma_{\rm R}$ should be taken at a scattering angle $\theta = \pi$, though any large angle may be used with an appropriately defined 'effective' energy (see Sec. III). This quasi-elastic barrier distribution is also sensitive to coupling effects, and behaves in a very similar way to that for fusion [8–10]. Note that $\sigma_{\rm fus}$ and $\sigma_{\rm qel}$ are in some sense complementary to one another, in that fusion corresponds to penetration of the potential barrier, whereas back scattering corresponds to reflection from the barrier.

In order to take account of coupling effects in the reaction process, the coupled-channels method is considered to be a standard approach [4,11]. Conventionally, only a few low-lying collective excitations, such as surface vibrations of spherical nuclei or rotations of nuclei with static deformations, have been taken into account. These coupled-channels analyses have successfully accounted for the strong enhancement of sub-barrier fusion cross sections as well as for the observed structures in the barrier distributions for many systems [4].

Nevertheless, there remain several challenging problems to be explored in the present coupled-channels approach. For instance, it has been a long-standing problem that a standard value of $a \sim 0.63$ fm for the surface diffuseness parameter of the real nuclear potential appears too small to account for fusion data, even though this value is required to fit scattering data [12,13]. This problem is also related [14–16] to the deviations of fusion cross sections at deep subbarrier energies from the predictions of standard coupled-channels calculations [17–20].

Another example is quasi-elastic scattering in the ^{20}Ne + ^{90,92}Zr systems [21]. For these systems, the experimental quasi-elastic barrier distributions exhibit significantly different behavior, that is, the barrier distribution for the ^{20}Ne + ^{92}Zr system shows a much more smeared structure than that for the ^{20}Ne + ^{90}Zr system. In contrast, the coupled-channels calculations that include the collective excitations in the ^{20}Ne and Zr isotopes, yield very similar barrier distributions for the two systems. In the calculations, the rotational excitations of the strongly deformed ^{20}Ne nucleus dominate the barrier structure, and the collective vibrational excitations in the Zr isotopes are found to play a minor role. Experimental data for the total transfer cross section at an energy near the Coulomb barrier have been found to be essentially the same [21], and the difference in the barrier distributions has been conjectured to originate from differences in the noncollective excitations in the two Zr isotopes. In fact, since the ^{92}Zr nucleus has two neutrons outside the $N = 50$ closed shell in ^{90}Zr, a larger number of noncollective excited states are present in the spectrum (for example, the number of known states up to 5 MeV is only 35 for ^{90}Zr but 87 for ^{92}Zr [22]).

The aim of this paper is to investigate whether the noncollective excitations of the ^{90,92}Zr isotopes can explain the observed differences in the quasi-elastic barrier distributions for the ^{20}Ne + ^{90,92}Zr systems, by explicitly taking them into account in large-scale coupled-channels calculations. In order to describe the noncollective excitations, we employ

the random-matrix model, which was originally introduced in the 1970s by Weidenmüller *et al.* in order to study deep-inelastic collisions [23–29]. In Ref. [30], we have shown that the noncollective excitations are not sensitive to how they are modeled and that the random-matrix method provides a good way to treat them when the relevant properties of the noncollective states are not well known (see also Refs. [31,32]). This justifies the use of the random-matrix model in the present analyses.

The paper is organized as follows. In Sec. II, we present the coupled-channels formalism and its various ingredients. In particular we detail the collective coupling parameters and the generation of the random-matrix, noncollective couplings that will be applied to the quasi-elastic scattering in the ^{20}Ne + ^{90,92}Zr systems. In Sec. III, we discuss the effect of the noncollective excitations on the corresponding quasi-elastic scattering cross sections, on the barrier distributions, and on the Q-value distributions. The paper is summarized in Sec. IV.

II. COUPLED-CHANNELS METHOD WITH NONCOLLECTIVE EXCITATION

A. Coupled-channels equations

The coupled-channels equations in the isocentrifugal approximation are given by [4],

$$\left[-\frac{\hbar^2}{2\mu}\frac{d^2}{dr^2} + \frac{J(J+1)\hbar^2}{2\mu r^2} + V_{\rm rel}(r) + \epsilon_n - E\right] u_n^J(r) + \sum_m V_{nm}(r) u_m^J(r) = 0, \quad (1)$$

where ϵ_n is the excitation energy for the nth channel and J is the total angular momentum. μ and $V_{\rm rel}(r)$ are the reduced mass and the optical potential for the relative motion, respectively. The coupling matrix elements, $V_{nm}(r)$, in Eq. (1) are evaluated as follows. For the couplings to the collective excitations, we compute the coupling matrix elements according to the collective model in the full-order coupling [4,11]. For the couplings to the noncollective excitations, on the other hand, we employ the random-matrix model [30]. Based on this model, we consider an ensemble of coupling matrix elements and require that their first moment satisfies

$$\overline{V_{nn'}^{II'}(r)} = 0, \quad (2)$$

while the second moment satisfies

$$\overline{V_{nn'}^{II'}(r) V_{n''n'''}^{I''I'''}(r')} = \{\delta_{nn''}\delta_{n'n'''}\delta_{II''}\delta_{I'I'''} + \delta_{nn'''}\delta_{n'n''}\delta_{II'''}\delta_{I'I''}\} \times \sqrt{(2I+1)(2I'+1)} \sum_\lambda \begin{pmatrix} I & \lambda & I' \\ 0 & 0 & 0 \end{pmatrix}^2 \times \alpha_\lambda(n, n'; I, I'; r, r'). \quad (3)$$

Here, the bars denote an ensemble average. I is the spin of the intrinsic state labeled by n, and α_λ is the coupling form factor.

In this paper, for simplicity, we take into account the coupling to noncollective states only from the ground state. This is similar to the linear coupling approximation. For the coupling form factor α_λ, we assume the following form:

$$\alpha_\lambda(n, 0; I, 0; r, r') = \frac{w_\lambda}{\sqrt{\rho(\epsilon_n)}} e^{-\frac{\epsilon_n^2}{2\Delta^2}} e^{-\frac{(r-r')^2}{2\sigma^2}} h(r)h(r'), \quad (4)$$

where $\rho(\epsilon_n)$ is the level density at excitation energy ϵ_n, and $(w_\lambda, \Delta, \sigma)$ are adjustable parameters. The appearance of the level density in the denominator of the form factor reflects the complexity of the noncollective states [26]. For the function $h(r)$, we assume that it is given by the derivative of our Woods-Saxon potential shape, that is,

$$h(r) = \frac{e^{(r-R)/a}}{[1+e^{(r-R)/a}]^2}, \quad (5)$$

as in the coupling matrix elements for the collective states in the linear-coupling approximation.

B. Potential parameters and the couplings to collective excited states

For the nuclear potential, we use the Woods-Saxon form with surface diffuseness parameter $a = 0.65$ fm and radius parameter $r_0 = 1.15$ fm for both systems. The depth V_0 is taken to be 55.0 MeV for ^{20}Ne + ^{90}Zr and 62.3 MeV for ^{20}Ne + ^{92}Zr. The resulting Coulomb barrier heights are $V_{\rm B} = 54.0$ MeV and 53.3 MeV, respectively.

As for the couplings in the ^{20}Ne nucleus, we consider the rotational states in the ground state band up to the 6^+ state with the deformation parameters $\beta_2 = 0.46$ and $\beta_4 = 0.27$. The octupole phonon state at 5.62 MeV is also included with $\beta_3 = 0.39$. For the couplings to the collective excited states in the ^{90}Zr nucleus, we take into account the vibrational 2^+ state at 2.18 MeV with $\beta_2 = 0.089$ and the 3^- state at 2.75 MeV with $\beta_3 = 0.211$ [39]. For the ^{92}Zr nucleus, we take into account the vibrational 2^+ state at 0.93 MeV with $\beta_2 = 0.103$ and the 3^- state at 2.34 MeV with $\beta_3 = 0.17$. For the quadrupole phonon, following Ref. [40], we use a slightly larger deformation parameter $\beta_2^{(\rm N)} = 0.144$ for the nuclear coupling. These collective excitations in the Zr isotopes are taken into account up to the two-phonon states, whereas the mutual excitations of the quadrupole and the octupole phonons are not included.

C. Couplings to noncollective excited states

The aim of this paper is to discuss the effect of noncollective excitations in the zirconium targets on the ^{20}Ne + ^{90,92}Zr reactions. We do not consider the noncollective excitations in the ^{20}Ne projectile, as there exist only a few noncollective states in the low-energy region in this light nucleus (for instance, the band heads for noncollective bands below 7 MeV are only the 2_1^- state at 4.97 MeV and 0_2^+ state at 6.73 MeV [41,42]). For the zirconium noncollective states, the excitation energies and spins are well known experimentally [22], but the deformation parameters (that is, the coupling strengths) are poorly known. We take, therefore, the experimental values of the excitation energies and spins, while we estimate the coupling matrix elements using the random-matrix model. Among the noncollective excited states, we take into account

TABLE I. Coefficients for $n = 0$–6 for the polynomial fits to the function $N(\epsilon)$ defined by Eq. (7). The units of a_n are MeV^{-n}.

Nucleus	a_0	a_1	a_2	a_3	a_4	a_5	a_6
^{90}Zr	199.2	182.5	−286.5	119.7	−22.65	2.057	−0.07278
^{92}Zr	63.79	540.7	−737.2	366.7	−87.00	10.07	−04589

only those with natural parity, given that both the projectile and the target nuclei are even-even nuclei. For the parameters in the random-matrix model, we use $\Delta = 7$ MeV, $\sigma = 4$ fm, and $w_\lambda = w = 200$ MeV$^{3/2}$. The values for Δ and σ are the same as those in Refs. [28,29], while the value for w, that determines the coupling strengths to the noncollective excited states, is chosen by fitting the experimental barrier distribution for the ^{20}Ne + ^{92}Zr system. The same values for the parameters are then used for the calculations in the ^{20}Ne + ^{90}Zr system, though of course the level density is different in that case.

In order to calculate the coupling matrix elements for the noncollective excitations, these level densities are required [see Eq. (4)], and in order to implement them in the coupled-channels calculations, we introduce a continuous level density as follows [30]. We first note that the level density is defined by

$$\rho(\epsilon) = \sum_n \delta(\epsilon - \epsilon_n), \tag{6}$$

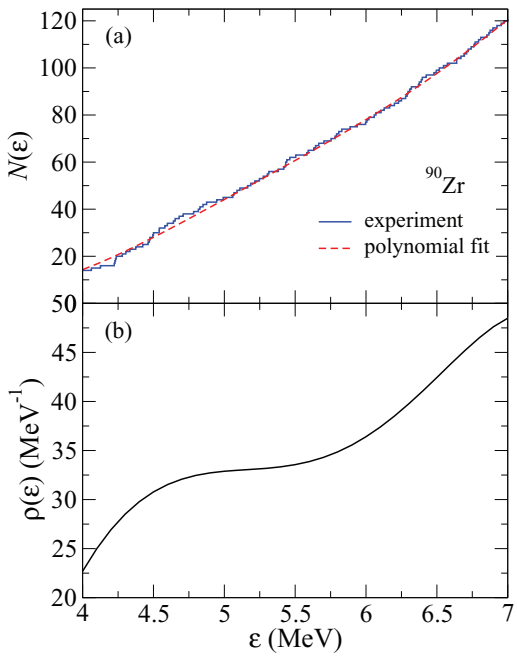

FIG. 1. (Color online) Upper panel: the number of levels of ^{90}Zr up to excitation energy ϵ as a function of ϵ. The histogram represents the experimental data [22], while the dashed line shows its fit with a sixth-order polynomial. Lower panel: the continuous level density obtained as the first derivative of the fitting function of the upper panel.

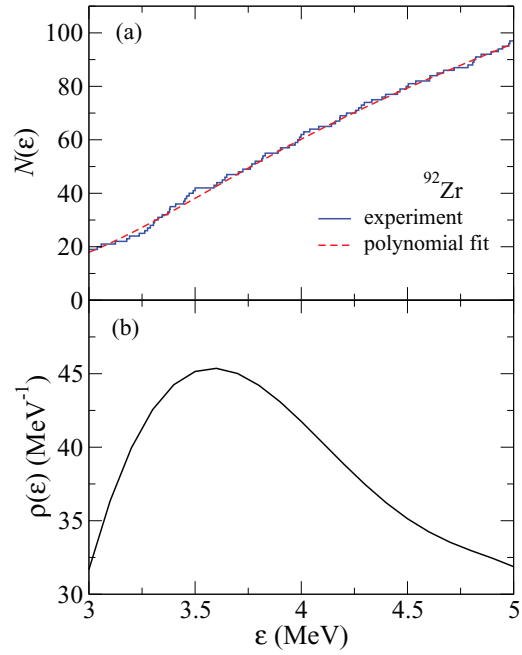

FIG. 2. (Color online) The same as Fig. 1 but for ^{92}Zr.

for a discrete spectrum. From the empirical level density $\rho(\epsilon)$, we then define the following function:

$$N(\epsilon) = \int_0^\epsilon \rho(\epsilon')d\epsilon' = \sum_n \theta(\epsilon - \epsilon_n). \tag{7}$$

This gives the number of levels up to an excitation energy ϵ. The solid lines in the upper panel of Figs. 1 and 2 show the experimental values for $N(\epsilon)$ for ^{90}Zr and ^{92}Zr, respectively. We next fit this function with a polynomial in ϵ. For ^{90}Zr, we fit $N(\epsilon)$ in the interval between 3 MeV and 8 MeV with a sixth-order polynomial $f(\epsilon) = \sum_{n=0}^{6} a_n \epsilon^n$. For ^{92}Zr, we fit $N(\epsilon)$ in the interval between 2.5 MeV and 6 MeV with a similar function. Values of the coefficients a_n are given in Table I. The dashed lines in the upper panels of Figs. 1 and 2 show the quality of the fits. We then obtain the continuous level densities by differentiating $f(\epsilon)$ with respect to ϵ. The resultant, continuous level densities for the two isotopes are shown in the lower panels of Figs. 1 and 2.

III. RESULTS

A. Quasi-elastic scattering cross sections and barrier distributions

Let us now solve the coupled-channels equations for the ^{20}Ne + ^{90,92}Zr systems and examine the effect of noncollective excitations on their quasi-elastic scattering. Figure 3 shows the quasi-elastic cross section and the quasi-elastic barrier distribution for the ^{20}Ne + ^{90}Zr system, whereas Fig. 4 shows the same functions for ^{20}Ne + ^{92}Zr. These quantities are plotted as a function of the effective energy defined by

$$E_{\rm eff} = 2E \frac{\sin(\theta_{\rm c.m.}/2)}{1 + \sin(\theta_{\rm c.m.}/2)}, \tag{8}$$

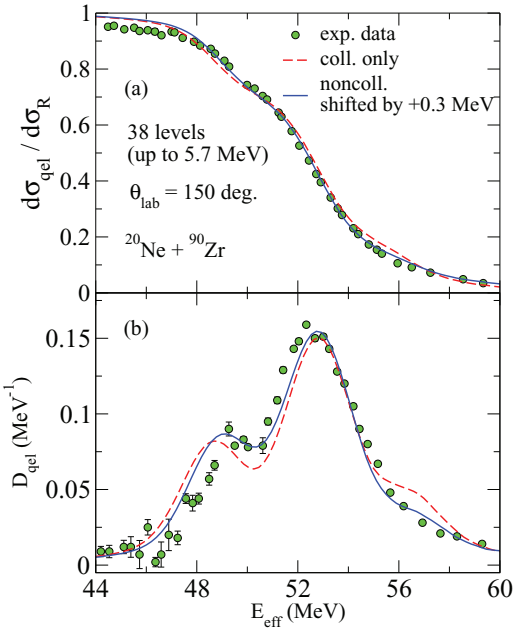

FIG. 3. (Color online) The quasi-elastic cross section (upper panel) and the quasi-elastic barrier distribution (lower panel) for the ^{20}Ne + ^{90}Zr system at the scattering angle $\theta_{\rm lab} = 150^\circ$. Dots represent the experimental data, taken from Ref. [21]. Dashed lines show the results obtained by including only collective excitations, while solid lines show the results including the noncollective excitations. The solid lines are shifted in energy by the amount shown in the figure in order to compensate for the trivial change of Coulomb barrier height due to the noncollective couplings.

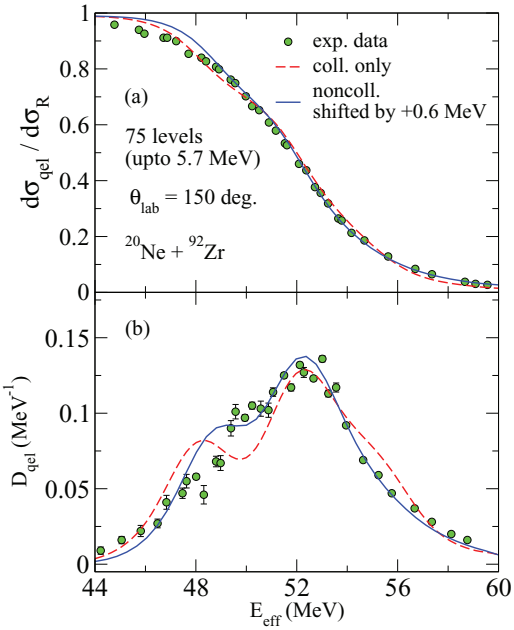

FIG. 4. (Color online) The same as Fig. 3 but for the ^{20}Ne + ^{92}Zr system.

where $\theta_{\rm c.m.}$ is the center-of-mass scattering angle. This quantity is introduced to map quasi-elastic cross sections at $\theta_{\rm c.m.}$ to their notional values at $\theta_{\rm c.m.} = \pi$, by correcting for the centrifugal energy of the corresponding classical Rutherford trajectory [8,9]. In both figures, the dots represent experimental data taken at $\theta_{\rm lab} = 150^\circ$ [21], while the dashed lines show the results that take account of only the collective excitations. The solid lines represent the results that take into account the noncollective excitations in addition to the collective ones. To this end, we include noncollective states up to 5.7 MeV; this corresponds to 38 levels in ^{90}Zr and 75 levels in ^{92}Zr. We have confirmed that the results do not change significantly if the noncollective states are truncated at higher excitation energies. Note that these results have been obtained with a single realization of the coupling matrix elements. In principle one should repeat the calculations many times with randomly generated matrix elements and take an ensemble average. However, we have verified in a smaller model space that the dispersion due to the randomness of these elements is sufficiently small that a single realization already yields reasonable results. Note also that the excitation energies of the noncollective states are relatively large, so that coupling to them leads to an adiabatic renormalization of the barrier [4,43]. We have therefore shifted the solid lines in energy by +0.3 and +0.6 MeV for the ^{20}Ne + ^{90}Zr and ^{20}Ne + ^{92}Zr systems, respectively, in order to compensate for this trivial modification of the barrier height.

For the ^{20}Ne + ^{90}Zr reaction, one sees that noncollective excitations do not alter the barrier distribution in a significant way, though the dip between the two main peaks is somewhat filled. In marked contrast, in the ^{20}Ne + ^{92}Zr reaction, the noncollective excitations almost completely fill this dip, leading to a much more smeared barrier distribution. Furthermore the overall width of the distribution becomes smaller in this case. These changes all lead to a much more satisfactory agreement with the experimental data. Moreover, we note that the noncollective excitations considerably improve the behavior around $E_{\rm eff} \sim 56$ MeV in both systems. In all these calculations, the same values for the parameters w, Δ, and σ of the random-matrix model are used. Therefore, any difference in the noncollective effects originates solely from the different level densities of these zirconium isotopes. That is, the effect of noncollective excitations is greater for ^{92}Zr since a larger number of noncollective states exist in the region of relatively low excitation energy. As noted above, this higher level density is due to the two extra neutrons outside the $N = 50$ closed neutron shell in ^{90}Zr.

Our calculations also indicate that the role of noncollective excitations in *fusion* barrier distributions is similar to that in the quasi-elastic barrier distributions. That is, the fusion barrier distribution for the ^{20}Ne + ^{92}Zr system is significantly altered due to the noncollective excitations, in a similar manner as in the corresponding quasi-elastic barrier distribution shown in Fig. 4, while the fusion barrier distribution for the ^{20}Ne + ^{90}Zr system is not affected much. This, of course, is rather expected since there is no reason why the different couplings for the two Zr isotopes should not affect the fusion and quasi-elastic barrier distributions in a different way. This suggests that one can indeed have a smoother fusion barrier distribution for the ^{20}Ne + ^{92}Zr system as compared to that for the ^{20}Ne + ^{90}Zr system.

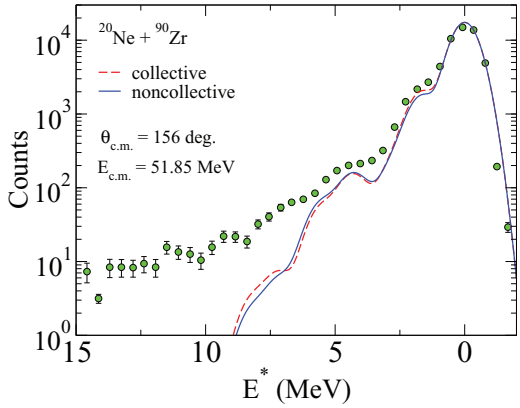

FIG. 5. (Color online) The Q-value distributions for the ^{20}Ne + ^{90}Zr system at a scattering angle $\theta_{c.m.} = 156^\circ$ and incident center-of-mass energy $E_{c.m.} = 51.85$ MeV. Experimental data are taken from Ref. [21]. The calculated results are smeared with a Gaussian function with a width of $\eta = 0.5$ MeV, and then normalized to the experimental elastic peak at $E^* = 0$.

The calculations shown in Figs. 3 and 4 still do not reproduce the quasi-elastic scattering cross sections at low energies around $E_{\rm eff} \sim 46$ MeV, despite the fact that the calculations agree well with the data at higher energies. We do not know the origin of this discrepancy, but other effects, such as α pick-up reactions, might play some role.

B. Q-value distribution

We next discuss the Q-value distribution, that is, the excitation energy spectra. Figures 5 and 6 show the Q-value distributions for the ^{20}Ne + ^{90}Zr and ^{20}Ne + ^{92}Zr systems, respectively. The meaning of each line is the same as in Figs. 3 and 4. The experimental data were taken at $\theta_{c.m.} = 156^\circ$ and $E_{c.m.} = 51.85$ MeV and do not include the transfer cross sections [21,44]. The theoretical Q-value distributions are evaluated at $E = 51.55$ and 51.25 MeV for the ^{20}Ne + ^{90}Zr and ^{20}Ne + ^{92}Zr systems, respectively, that is, at those energies corresponding to $E_{c.m.} = 51.85$ MeV after the energy shifts

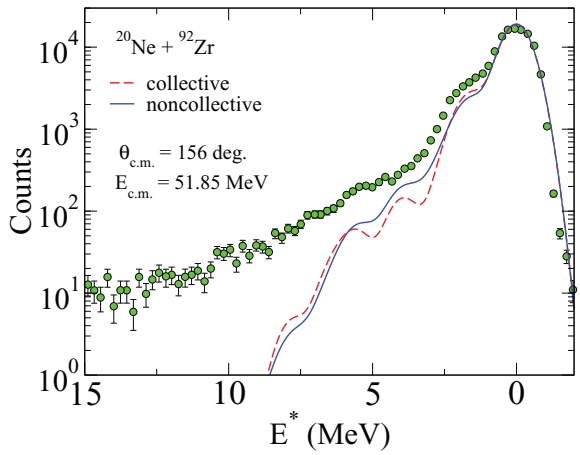

FIG. 6. (Color online) The same as Fig. 5, but for the ^{20}Ne + ^{92}Zr system. Experimental data are from Refs. [21,44].

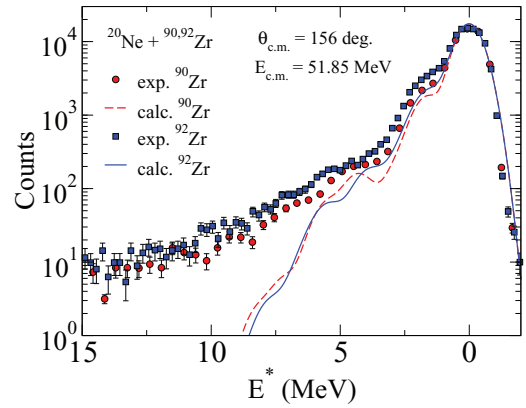

FIG. 7. (Color online) Comparison of the Q-value distributions for the ^{20}Ne + ^{90}Zr and ^{20}Ne + ^{92}Zr systems. The circles and the dashed line show, respectively,the experimental data and the calculated result for the ^{20}Ne + ^{90}Zr system, while the squares and the solid line represent the ^{20}Ne + ^{92}Zr system.

indicated in Figs. 3 and 4 are taken into account. They are obtained by summing over the different channels as follows:

$$F(E^*) \propto \sum_n \frac{d\sigma_n}{d\Omega} \frac{1}{\sqrt{2\pi}\,\eta} e^{-\frac{(E^*-\epsilon_n)^2}{2\eta^2}}, \qquad (9)$$

that is, we smear with a Gaussian function of width η to simulate the experimental energy resolution. The normalization factor and the value of the width ($\eta = 0.5$ MeV) are determined so that the elastic peak in the experimental Q-value distribution is reproduced.

One can see that the noncollective excitations affect little the Q-value distribution at this incident energy for either system. For ^{20}Ne + ^{90}Zr, the calculation reasonably reproduces the data up to about $E^* = 5$ MeV, although it underestimates the experimental data at higher energies due to the truncation of the noncollective states in our calculations. For the ^{20}Ne + ^{92}Zr system, the noncollective excitations somewhat enhance the contribution from the inelastic channels between about 3 to 6 MeV, and the experimental data are reasonably well reproduced up to 4 MeV.

Figure 7 compares the Q-value distributions for the two systems. The circles and the dashed lines are for the ^{20}Ne + ^{90}Zr system, while the squares and the solid lines are for the ^{20}Ne + ^{90}Zr system. They are all normalized to the height of the elastic peak in the experimental data for the ^{20}Ne + ^{90}Zr system. One can see that the experimental Q-value distributions are similar for both the systems, and are well reflected by the present coupled-channels calculations.

This might appear surprising given that there is a large difference between the two measured quasi-elastic barrier distributions (see Fig. 3 and 4). This does not necessarily mean that the noncollective excitations do not play an important role in the Q-value distribution, however. In order to demonstrate this, we show in Figs. 8 and 9 the energy dependence of the Q-value distribution obtained at different incident energies from 40 MeV to 60 MeV for the ^{20}Ne + ^{90}Zr and ^{20}Ne + ^{92}Zr systems. The dashed peaks show contributions from the collective channels, while the solid peaks show the

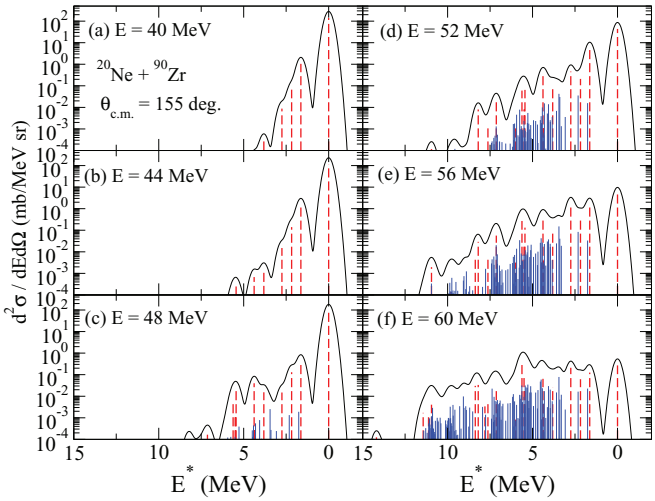

FIG. 8. (Color online) The energy dependence of the Q-value distribution for the ^{20}Ne + ^{90}Zr system. The dashed and the solid peaks show the contributions from the collective and the non-collective excitations, respectively. The solid lines are obtained by smearing the spectra with a Gaussian function of width 0.2 MeV.

contributions from the noncollective channels. We also show envelopes of the peaks by the solid lines, that are obtained by smearing with a Gaussian function of width 0.2 MeV. For both systems, the contribution from the elastic channel and the collective excitations is dominant at energies below the barrier, while the contribution from the noncollective excitations becomes more important as the incident energy increases. This tendency was also observed in our previous calculations for the ^{16}O + ^{208}Pb system [32] (see Refs. [45–47] for the corresponding experimental data). We note again that in the present systems, the noncollective excitations contribute more in the ^{20}Ne + ^{92}Zr system, and it would therefore be interesting to compare the experimental Q-value spectra for the two systems at higher energies than studied in Ref. [21]. There the effect of noncollective excitations might be seen more clearly.

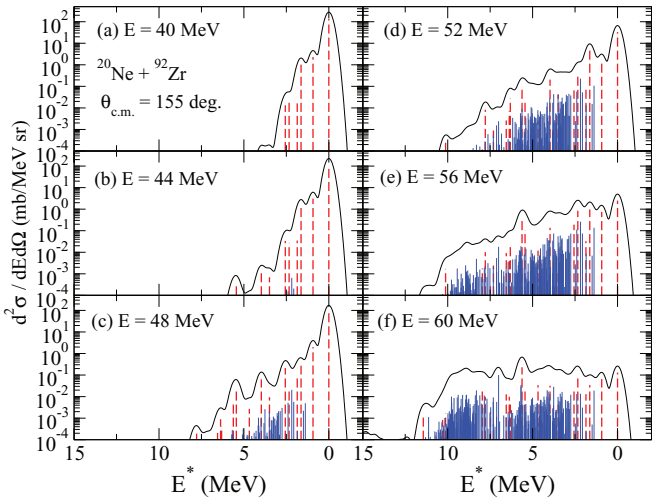

FIG. 9. (Color online) Same as Fig. 8, but for ^{20}Ne + ^{92}Zr.

IV. SUMMARY

We have investigated the role of noncollective excitations of Zr isotopes in the ^{20}Ne + ^{90,92}Zr reactions. This was motivated by recent quasi-elastic scattering experiments for these systems, in which the conventional coupled-channels calculations could not explain the difference between the two quasi-elastic barrier distributions. In this paper, we have employed the random-matrix model to generate appropriate couplings to noncollective states, enabling us to include these excitations in our coupled-channels calculations.

The results indicate that these excitations fill in the dip between the two main peaks in the barrier distribution for the ^{20}Ne + ^{92}Zr system, considerably smearing its peak structure. In contrast, the effect is much smaller for ^{20}Ne + ^{90}Zr, and the peak structure is not greatly affected by the inclusion of the noncollective excitations. The difference arises solely from the different level densities in these Zr isotopes. That is, the number of low-lying, non-collective states is much larger in ^{92}Zr than in ^{90}Zr. In both systems, the agreement with the experimental data for the quasi-elastic scattering cross sections and the barrier distribution is improved by the inclusion of these excitations.

We have also calculated the Q-value distribution for ^{20}Ne + ^{90,92}Zr scattering. At an incident energy $E_{\rm c.m.}$ = 51.85 MeV, where experimental data exist, our calculations indicate that the contribution from the noncollective excitations is relatively small, even in the ^{20}Ne + ^{92}Zr system. In fact, the data show that the Q-value distributions do not differ significantly at this energy, a result consistent with our calculations. We have also calculated the energy dependence of the Q-value distribution for both systems, and have found that the contribution from the noncollective excitations becomes more important as the incident energy increases. A similar tendency has been observed experimentally in the ^{16}O + ^{208}Pb system.

Noncollective excitations are expected to become more important as the mass number increases. (Notice that the effect of noncollective excitations appear to be larger in the ^{16}O + ^{208}Pb reaction [32] than in the ^{20}Ne + ^{90}Zr reaction despite the fact that both ^{208}Pb and ^{90}Zr are closed-shell nuclei. This is partly because the effect is somewhat amplified in the former due to the larger charge product.) In this respect, we mention that the random-matrix model employed in this paper may be useful for the study of heavy-ion, deep-inelastic collisions, where a large number of noncollective excitations play a role. Even though the random-matrix model has been applied to deep-inelastic collisions in the 1970s by Weidenmüller *et al.*, a major difference in our work is that we have solved the coupled-channels equations quantum mechanically; this is essential for low-energy heavy-ion reactions. An interesting future problem would be to develop a more quantum mechanical approach for the deep-inelastic processes, still based on the random-matrix model.

ACKNOWLEDGMENTS

We thank E. Piasecki for useful discussions. This work was supported by the Global COE Program "Weaving Science

Web beyond Particle-Matter Hierarchy" at Tohoku University, and by the Japanese Ministry of Education, Culture, Sports, Science and Technology by Grant-in-Aid for Scientific Research under program no. (C) 22540262.

[1] C. H. Dasso, S. Landowne, and A. Winther, Nucl. Phys. A **405**, 381 (1983); **407**, 221 (1983).
[2] M. Dasgupta, D. J. Hinde, N. Rowley, and A. M. Stefanini, Annu. Rev. Nucl. Part. Sci. **48**, 401 (1998).
[3] A. B. Balantekin and N. Takigawa, Rev. Mod. Phys. **70**, 77 (1998).
[4] K. Hagino and N. Takigawa, Prog. Theor. Phys. **128**, 1001 (2012).
[5] N. Rowley, G. R. Satchler, and P. H. Stelson, Phys. Lett. B **254**, 25 (1991).
[6] J. R. Leigh *et al.*, Phys. Rev. C **52**, 3151 (1995).
[7] J. R. Leigh, N. Rowley, R. C. Lemmon, D. J. Hinde, J. O. Newton, J. X. Wei, J. C. Mein, C. R. Morton, S. Kuyucak, and A. T. Kruppa, Phys. Rev. C **47**, R437 (1993).
[8] H. Timmers, J. R. Leigh, M. Dasgupta, D. J. Hinde, R. C. Lemmon, J. C. Mein, C. R. Morton, J. O. Newton, and N. Rowley, Nucl. Phys. A **584**, 190 (1995).
[9] K. Hagino and N. Rowley, Phys. Rev. C **69**, 054610 (2004).
[10] Muhammad Zamrun F. and K. Hagino, Phys. Rev. C **77**, 014606 (2008).
[11] K. Hagino, N. Rowley, and A. T. Kruppa, Comput. Phys. Commun. **123**, 143 (1999).
[12] A. Mukherjee, D. J. Hinde, M. Dasgupta, K. Hagino, J. O. Newton, and R. D. Butt, Phys. Rev. C **75**, 044608 (2007).
[13] J. O. Newton, R. D. Butt, M. Dasgupta, D. J. Hinde, I. I. Gontchar, C. R. Morton, and K. Hagino, Phys. Lett. B **586**, 219 (2004); Phys. Rev. C **70**, 024605 (2004).
[14] K. Hagino, N. Rowley, and M. Dasgupta, Phys. Rev. C **67**, 054603 (2003).
[15] T. Ichikawa, K. Hagino, and A. Iwamoto, Phys. Rev. Lett. **103**, 202701 (2009); Phys. Rev. C **75**, 064612 (2007); **75**, 057603 (2007).
[16] S. Misicu and H. Esbensen, Phys. Rev. Lett. **96**, 112701 (2006); Phys. Rev. C **75**, 034606 (2007).
[17] C. L. Jiang, H. Esbensen, K. E. Rehm, B. B. Back, R. V. F. Janssens, J. A. Caggiano, P. Collon, J. Greene, A. M. Heinz, D. J. Henderson, I. Nishinaka, T. O. Pennington, and D. Seweryniak, Phys. Rev. Lett. **89**, 052701 (2002); Phys. Rev. C **79**, 044601 (2009), and references therein.
[18] C. L. Jiang, K. E. Rehm, R. V. F. Janssens, H. Esbensen, I. Ahmad, B. B. Back, P. Collon, C. N. Davids, J. P. Greene, D. J. Henderson, G. Mukherjee, R. C. Pardo, M. Paul, T. O. Pennington, D. Seweryniak, S. Sinha, and Z. Zhou, Phys. Rev. Lett. **93**, 012701 (2004).
[19] M. Dasgupta, D. J. Hinde, A. Diaz-Torres, B. Bouriquet, C. I. Low, G. J. Milburn, and J. O. Newton, Phys. Rev. Lett. **99**, 192701 (2007).
[20] A. M. Stefanini *et al.*, Phys. Rev. C **78**, 044607 (2008); Phys. Lett. B **679**, 95 (2009).
[21] E. Piasecki, Ł. Świderski, W. Gawlikowicz, J. Jastrzębski, N. Keeley, M. Kisieliński, S. Kliczewski, A. Kordyasz, M. Kowalczyk, S. Khlebnikov, E. Koshchiy, E. Kozulin, T. Krogulski, T. Loktev, M. Mutterer, K. Piasecki, A. Piórkowska, K. Rusek, A. Staudt, M. Sillanpää, S. Smirnov, I. Strojek, G. Tiourin, W. H. Trzaska, A. Trzcińska, K. Hagino, and N. Rowley, Phys. Rev. C **80**, 054613 (2009).
[22] Brookhaven National Laboratory, Evaluated Nuclear Structure Data File, http://www.nndc.bnl.gov/ensdf/, and references therein.
[23] C. M. Ko, H. J. Pirner, and H. A. Weidenmüller, Phys. Lett. B **62**, 248 (1976).
[24] D. Agassi, H. A. Weidenmüller, and C. M. Ko, Phys. Lett. B **73**, 284 (1978).
[25] B. R. Barrett, S. Shlomo, and H. A. Weidenmüller, Phys. Rev. C **17**, 544 (1978).
[26] D. Agassi, C. M. Ko, and H. A. Weidenmüller, Ann. Phys. (NY) **107**, 140 (1977).
[27] C. M. Ko, D. Agassi, and H. A. Weidenmüller, Ann. Phys. (NY) **117**, 237 (1979).
[28] D. Agassi, C. M. Ko, and H. A. Weidenmüller, Ann. Phys. (NY) **117**, 407 (1979).
[29] D. Agassi, C. M. Ko, and H. A. Weidenmüller, Phys. Rev. C **18**, 223 (1978).
[30] S. Yusa, K. Hagino, and N. Rowley, arXiv:1308.6418.
[31] S. Yusa, K. Hagino, and N. Rowley, Phys. Rev. C **82**, 024606 (2010).
[32] S. Yusa, K. Hagino, and N. Rowley, Phys. Rev. C **85**, 054601 (2012).
[33] R. Lindsay and N. Rowley, J. Phys. G **10**, 805 (1984).
[34] M. A. Nagarajan, N. Rowley, and R. Lindsay, J. Phys. G **12**, 529 (1986).
[35] M. A. Nagarajan, A. B. Balantekin, and N. Takigawa, Phys. Rev. C **34**, 894 (1986).
[36] H. Esbensen, S. Landowne, and C. Price, Phys. Rev. C **36**, 1216 (1987); **36**, 2359 (1987).
[37] O. Tanimura, Phys. Rev. C **35**, 1600 (1987); Z. Phys. A **327**, 413 (1987).
[38] J. Gomez-Camacho, M. V. Andres, and M. A. Nagarajan, Nucl. Phys. A **580**, 156 (1994).
[39] S. Kalkal *et al.*, Phys. Rev. C **81**, 044610 (2010).
[40] J. O. Newton, C. R. Morton, M. Dasgupta, J. R. Leigh, J. C. Mein, D. J. Hinde, and H. Timmers, and K. Hagino, Phys. Rev. C **64**, 064608 (2001).
[41] Y. Fujiwara, Prog. Theo. Phys. **62**, 122 (1979).
[42] M. Kimura, Phys. Rev. C **69**, 044319 (2004).
[43] N. Takigawa, K. Hagino, M. Abe, and A. B. Balantekin, Phys. Rev. C **49**, 2630 (1994).
[44] E. Piasecki (private communications).
[45] M. Evers, M. Dasgupta, D. J. Hinde, L. R. Gasques, M. L. Brown, R. Rafiei, and R. G. Thomas, Phys. Rev. C **78**, 034614 (2008).
[46] C. J. Lin, H. M. Jia, H. Q. Zhang, F. Yang, X. X. Xu, F. Jia, Z. H. Liu, and K. Hagino, Phys. Rev. C **79**, 064603 (2009).
[47] M. Evers, M. Dasgupta, D. J. Hinde, D. H. Luong, R. Rafiei, R. du Rietz, and C. Simenel, Phys. Rev. C **84**, 054614 (2011).